Fracture Mechanics of Concrete Structures
Proceedings FRAMCOS-3
AEDIFICATIO Publishers, D-79104 Freiburg, Germany

EXPERIMENTAL AND NUMERICAL EVALUATION OF GRAVITY DAM MODEL FAILURE LIFETIME

F. Barpi, S. Valente
Department of Structural Engineering, Politecnico di Torino, Italy
G. Ferrara
E.N.E.L.–C.R.I.S., Milano, Italy
L. Imperato
I.S.M.E.S., Seriate (Bergamo), Italy

Abstract
Three scaled-down (1:40) models of a gravity dam are subjected to an equivalent hydraulic and dead weight loading. An initial notch in the upstream side propagates during the loading towards the foundation. After the peak value, the testing machine switches from C.M.O.D. control to load control and executes three steps: unloading, reloading and constant load until failure. A numerical simulation of the experiments is carried out using a time-dependent cohesive crack model in Mixed-mode conditions. The structural behaviour of the models, in terms of total load, displacements and failure lifetime are reproduced by the finite element idealisation in a satisfactory manner.
Key words: Cohesive model, concrete, crack, creep, dam, fracture

1 Introduction

Creep induced crack propagation in concrete structures can be analysed within the framework of the cohesive crack model, a well established approach to the fracture mechanics of quasi-brittle materials (Barenblatt 1959; Dugdale 1960; Hillerborg 1976).

According to this model, the process zone can be represented as an extended portion of the real crack, called fictitious crack, where the material, albeit damaged, can still transfer stresses which are a decreasing

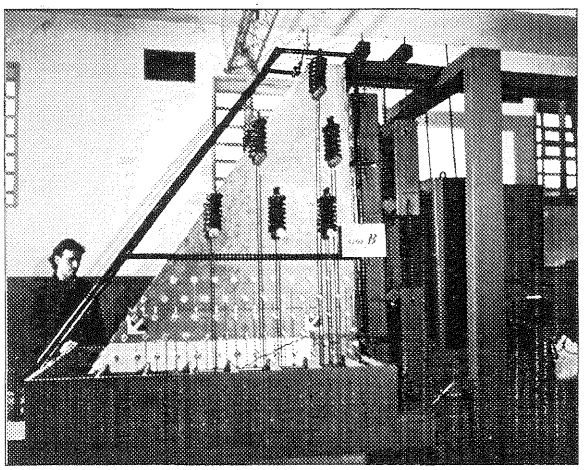

Fig. 1: Dam model testing equipment

function of the crack opening displacement.

This approach may be extended to take into account the time dependent behaviour of concrete in the process zone (Zhou 1992). The latter can be ascribed to the interaction and growth of the microcracks, a phenomenon which, for high constant load levels, turns out to be predominant over linear viscoelastic creep in the bulk material (Bazant and Xiang 1997).

2 Loading procedure

The experimental tests described in this paper can be grouped as follows:

A: stable tensile tests performed on cylindrical specimens, 10 cm in diameter and 20 cm high, with a 1 cm deep notch,

B: tests on pre-notched gravity dam models (Fig. 1). The geometric scale ratio between model and prototype was assumed to be S_ℓ = 1:40 (2.40 m (dam model height)/ 96 m (real dam height)). The scale adopted for density was $S_\rho = 1$, while the scale for stresses was $S_\sigma = 1$ (same value for both the model and the prototype). Having established the scales of two independent quantities (length and stress), the scales of the other quantities playing a role in static problems are determined according to Buckingham's Theorem. Applying this theorem, we get the scale of volume forces as $S_g = S_\sigma / (S_\rho\, S_\ell) = 40$. For this reason, it was necessary to simulate a dead weight increment (40 times) by means of a system of discrete vertical forces. The total volume of the model was subdivided into elementary portions and the equivalent forces to be applied were estimated. In order to check each vertical force applied, a spring-dynamometer is used. As shown in Fig. 1, each dynamometer

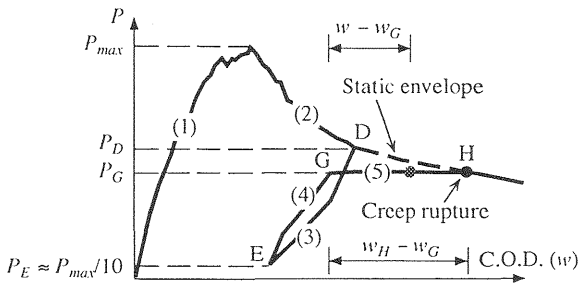

Fig. 2: Creep test procedure

is connected to a steel framework placed under the foundation of the dam. In order to disturb the static behaviour of the model as little as possible, in the fracture zone the vertical forces are applied through glued metallic plates.

Type A tests were performed at the E.N.E.L.–C.R.I.S. laboratories of Milan (Carpinteri et al. 1995, 1997), type B tests at the I.S.M.E.S. laboratories of Bergamo (Barpi and Valente 1996; Barpi et al. 1997a,b).

The same loading procedure, consisting of the following five stages, was used in both cases (Fig. 2):

1. C.M.O.D. (Crack Mouth Opening Displacement)-controlled loading from zero to the maximum value (P_{max}),
2. C.M.O.D.-controlled softening to point D,
3. P-controlled unloading to point E ($P_E \approx P_{max}/10$),
4. P-controlled reloading up to point G,
5. By keeping the load constant ($P = P_G$), we wait until specimen failure. Since this stage is started after reaching the peak load (P_{max}), this is known as the post-peak test.

3 Static properties of concrete

The specimens for static and creep tests were prepared together with the three dam models. The specimens and the models were stored at 20° C and 95% relative humidity and tested 8 months after the batch. Mean compressive strength was measured on six 15×15×15 cm cubes, Young's modulus on two 15×15×60 cm prisms, fracture energy was determined according RILEM recommendation through three-point bending tests, and tensile strength through type A tests. Mean static concrete properties are summarised in Table 1. The numerical simulations were performed on the basis of the properties listed in Table 1, assuming a Poisson's ratio of 0.1.

Table 1. Static properties of concrete

Maximum aggregate size Φ_{max} (mm)	Mean compressive strength (MPa)	Mean Young's modulus (GPa)	Mean fracture energy (N/m)	Mean tensile strength (MPa)
3.15	32	22.1	96.55	1.950
12	28	28.0	141.15	2.375
25	35	35.2	121.49	2.885

4 Unloading and reloading stages

In order to determine the state of stress in the fictitious process zone (F.P.Z.), it proves necessary to resort to a constitutive law for the unloading and reloading stages. As suggested in Barpi et al. (1998b), the numerical simulations were performed by using the Focal Point Model (Yankelevsky and Reinhardt 1989). For each cohesive element, the entire potential unloading polygonal turns out to be defined as soon as its initial point becomes known (Fig. 2). The same applies to the potential reloading polygonal originating from the point E.

5 Creep properties of concrete

During the constant load (P_G) stage of stable tensile tests, it is assumed that the tensile stress (σ_G) is the same at all points of the process zone and does not vary over time. The creep law adopted is the one proposed by Carpinteri et al. (1995, 1997), which is based on the following observations concerning type A tests:

- For the three concrete types analysed, the relationship between the load

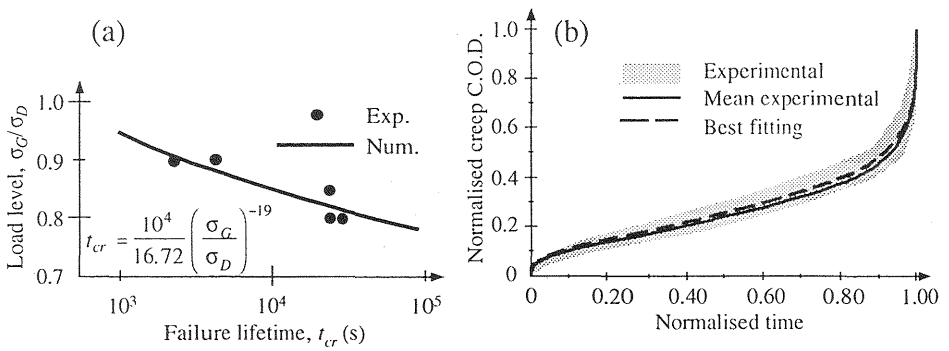

Fig. 3: Creep behaviour of concrete (Φ_{max} = 25 mm)

level, σ_G/σ_D, and failure lifetime, t_{cr}, can be best fitted by a power law, as shown in Fig. 3a.

- Figure 3b shows the normalised creep C.O.D. (defined as $w^c/w^c_{ult} = (w - w_G)/(w_H - w_G)$, see Fig. 2) vs. normalised time (t/t_{cr}) curves. For each type of concrete, the difference between such curves at different load levels (P_G/P_D) turned out to be not greater than the difference between different tests at the same level. As a result, this relationship was taken to be unique.

The best fitting curves shown in Fig. 3b were obtained by assuming creep related C.O.D. rate ($\dot{w}^c$) to depend on three terms, relating to primary, secondary and tertiary stage.

The two previous observations lead to the following creep laws, which were used in the numerical simulations:

$$\frac{\dot{w}^c}{w^c_{ult}} = \frac{9.71}{10^3}\left(\frac{\sigma_G}{\sigma_D}\right)^{27}\left(0.45 + 12\left(\frac{w^c}{w^c_{ult}}\right)^5 + 35\exp\left(-50\frac{w^c}{w^c_{ult}}\right)\right), \quad \Phi_{max} = 3.15\ \text{mm}, \quad (1a)$$

$$\frac{\dot{w}^c}{w^c_{ult}} = \frac{6.90}{10^3}\left(\frac{\sigma_G}{\sigma_D}\right)^{26}\left(0.40 + 25\left(\frac{w^c}{w^c_{ult}}\right)^5 + 9\exp\left(-50\frac{w^c}{w^c_{ult}}\right)\right), \quad \Phi_{max} = 12\ \text{mm}, \quad (1b)$$

$$\frac{\dot{w}^c}{w^c_{ult}} = \frac{16.72}{10^4}\left(\frac{\sigma_G}{\sigma_D}\right)^{19}\left(0.35 + 32\left(\frac{w^c}{w^c_{ult}}\right)^5 + 15\exp\left(-50\frac{w^c}{w^c_{ult}}\right)\right), \quad \Phi_{max} = 25\ \text{mm}. \quad (1c)$$

In this manner it becomes possible to characterise the time-dependent behaviour of the process zone forming in a given type of concrete.

6 Constant load stage

During stage 5, the external load is kept constant and because of the relaxation of the process zone the stress path extends from point G to the static envelope. In the numerical simulations, the latter was simulated by means of Petersson's (1981) bilinear curve. According to the integration procedure proposed by Zhou (1992), any time increment can be broken down into two steps (Fig. 4)

(a) during time dt, w is kept constant, and a relaxation stress $d\sigma^R = F\ \dot{w}^c\ dt$ develops in the process zone ($\dot{w}^c$ is given by Eqn (1)),
(b) the reduction in the closing cohesive stresses acting on the edges of the fictitious crack causes an increase in crack opening, dw, and an increase in stress, dσ^I, in each cohesive element.

In stage 5, unlike stages 3 and 4, the stress path does not depend solely on the definition of its initial point G, but also on the evolution of displacements over time. In Fig. 4 the sequence of steps is magnified for the sake of clarity. Upon reaching the static envelope, the stress path is forced to follow it ($\dot{w} > 0$).

7 The cohesive crack model

Under high level sustained load, creep outside the process zone can be neglected compared to creep in the process zone (Bazant and Xiang 1997). Therefore, the constitutive law for the continuum is linear elastic, time independent. According to the finite element method, keeping in mind that the constitutive law for the fictitious crack is assumed to be piece-wise linear, by taking the unknowns to be the n nodal displacements, $\boldsymbol{u}$, it is possible to write the equilibrium condition, for each solution increment, through the virtual work equation as follows (Carpinteri and Valente 1988; Bocca et al. 1991; Carpinteri et al. 1992; Valente et al. 1994; Barpi et al. 1997a,b; Barpi and Valente 1996, 1998a,b):

$$(K_T + C_T)\, \mathrm{d}\boldsymbol{u} = \mathrm{d}\lambda\, \boldsymbol{P} + \mathrm{d}t\, \boldsymbol{Q}\,, \tag{2}$$

where:

K_T: positive definite tangential stiffness matrix, containing contributions from linear elastic elements and possible contributions from cohesive elements with values (σ, w) inside the static envelope (stages 3, 4 and 5),

C_T: negative definite tangential stiffness matrix, containing contributions from cohesive elements with values (σ, w) on the static envelope,

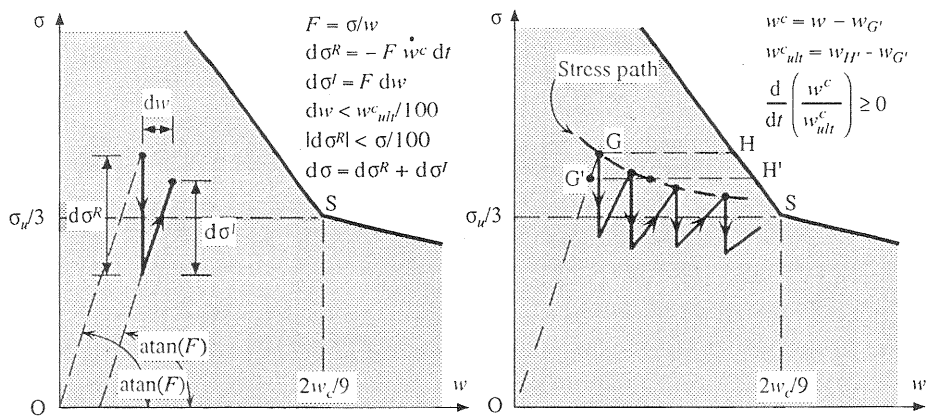

Fig. 4: Stress path due to creep during the constant load stage

$\boldsymbol{P}$: vector of incremental load normalised in order to obtain $\sum P_i^2 = 1$,
$d\lambda$: maximum load multiplier which is compatible will all active limits. For example, no stress increment can go through point S of Fig. 4 within a single step, and at least two steps are necessary, since matrix $\boldsymbol{C}_T$ has to be reassembled,
$\boldsymbol{Q}$: vector of unbalanced load (or pseudo-load) due to relaxation in the process zone, related to a unitary time increment,
dt: max. time increment compatible with all limits active (see also $d\lambda$).

The displacements, $\boldsymbol{u}$, are related to the process zone, and to the loading points. For purposes of numerical efficiency, the remaining displacements are statically condensed. The nodes on the crack are split and connected by a two-node element orthogonal to the crack. These elements, which are mutually independent, follow the constitutive law for the process zone.

During stages 1, 2, 3 and 4, the behaviour of the material is assumed to be time independent ($\boldsymbol{Q} = \boldsymbol{0}$), the external load changes ($d\lambda \neq 0$), and $dt = 0$. On the contrary, during stage 5, the behaviour of the process zone is assumed to be time dependent ($\boldsymbol{Q} \neq \boldsymbol{0}$), the external load is kept constant ($d\lambda = 0$) and $dt \neq 0$. The elements having (σ, w) on the static envelope, together with those arising from the growth of the fictitious crack, contribute to matrix $\mathbf{C}_T$ ($d\sigma/dw < 0$); when their number becomes significant, the $\boldsymbol{K}_T + \mathbf{C}_T$ matrix loses its characteristic of being positive definite and the constant load may no longer be sustained. This condition determines the failure lifetime of the structure (t_{cr}).

8 Gravity dam model test simulation

Details of the finite element mesh and the constitutive law for the real crack and the notch during the reclosing stages are given in Barpi and Valente (1996). Figs. 5a-f show that the numerical and experimental results are in good agreement in terms of equivalent hydraulic load, C.M.O.D. and failure lifetime. C.M.O.D. vs. time diagrams and crack trajectories are given by Barpi and Valente (1996). In the tests illustrated in Figs. 5b, 5d and 5f, model failure occurred at the reloading stage. Therefore the experimental failure lifetime is computed from the test starting time. Figs. 5b, 5d and 5f show that about 50% of peak load is required to balance the dead weight so as obtain C.M.O.D = 0, along the first loading branch. Therefore the P_G/P_D ratios presented in Figs. 5a, 5c, 5e are not comparable with the ratios obtained in bending and tensile tests. Unlike Mode I conditions, these testing conditions call for several remeshing steps during stage 5, which cause perturbations in the time integration process resulting in an appreciable (albeit acceptable) degree of scatter in the numerical results (Figs. 5a, 5c and 5e).

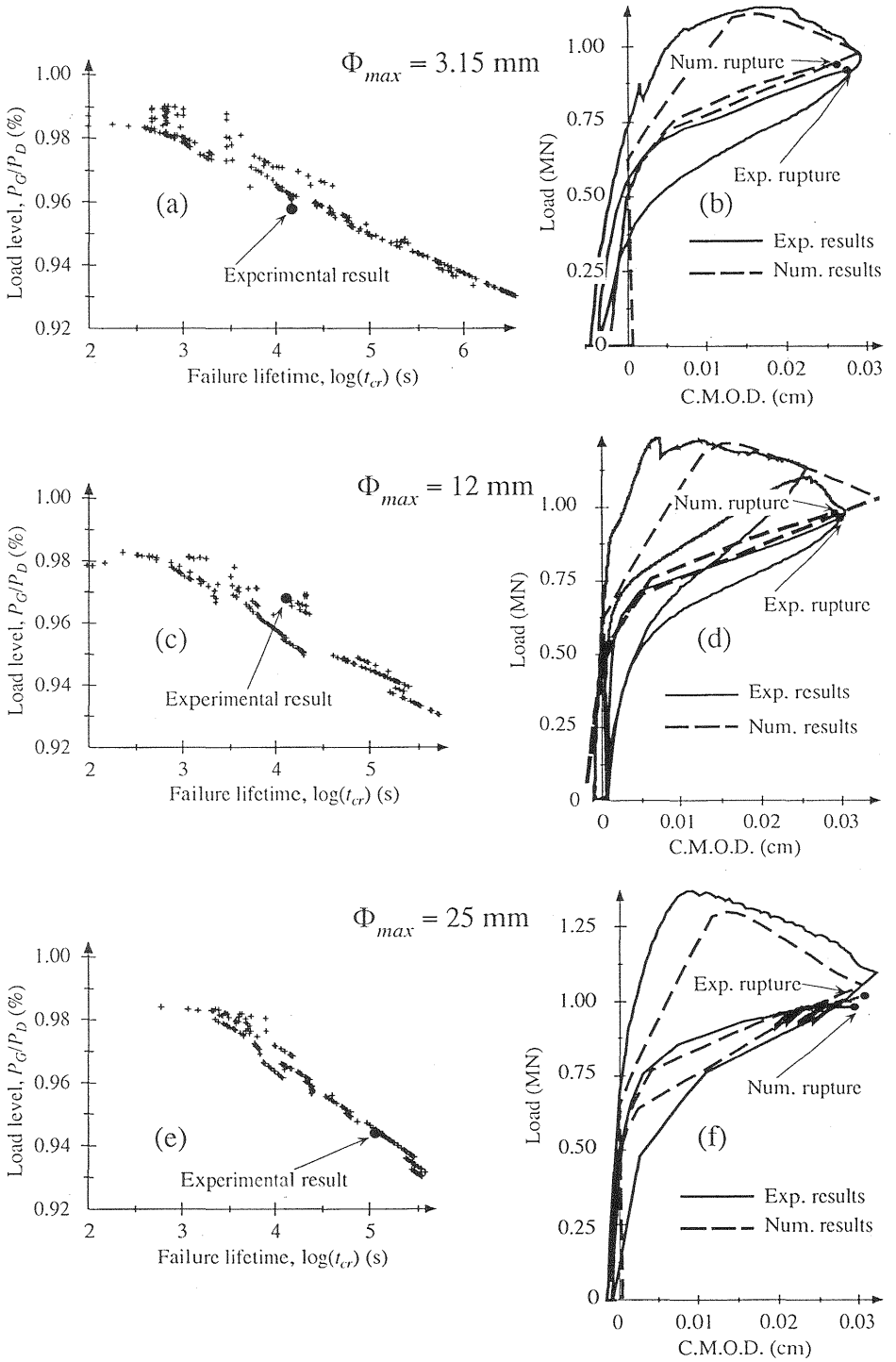

Fig. 5: Load vs. Crack Mouth Opening Displacement and load level vs. failure lifetime (dam models)

9 Conclusions

1. The structural behaviour of three dam models, in terms of equivalent hydraulic load, C.M.O.D. and failure lifetime are reproduced by the finite element idealisation in a satisfactory manner.
2. This is obtained by characterising the time dependent behaviour of the process zone through stable tensile tests and by introducing the properties worked out in this manner into the cohesive crack model.
3. In Mixed-mode conditions, the remeshing step behaves as a perturbation of the time integration process. This is the reason for the scatter in the numerical results obtained for failure lifetime vs. load level (Figs. 5a, 5c and 5e).
4. This degree of scatter is lower than is observed in fields where numerous experimental (tensile and bending) test results are available (see, for example, Fig. 3a).
5. Direct tensile tests and three-point bending tests show that collapse occurs when the load vs. C.M.O.D. path reaches the corresponding static curve (static envelope), see point H of Fig. 2. On the contrary, experimental and numerical results obtained on three gravity dam models show that creep failure occurs when the path is still well inside the static envelope, as shown by the points denoted as "exp. rupture" and "num. rupture" in Figs. 5b, 5d and 5f.

10 References

Barenblatt, G.I. (1959) The formation of equilibrium cracks during brittle fracture: general ideas and hypotheses. Axially-symmetric cracks. **J. Appl. Math. Mech.**, 23, 622-636.

Barpi, F. and Valente, S. (1996) Time Induced Crack Propagation in Concrete Structures: Cohesive Crack Model in Mixed-mode Conditions, Politecnico di Torino, Structural Engineering Department, Research Report A845/95.

Barpi, F., Chillè, F., Imperato, L. and Valente, S. (1997a) Creep induced cohesive crack propagation in mixed mode, in **Proceedings of the I.U.T.A.M. Symposium on Non–Linear Singularities in Deformation and Flow** (ed. D. Durban), in press.

Barpi, F., Chillè, F., Imperato, L. and Valente, S. (1997b) Failure lifetime prediction of cracked concrete structures. Paper accepted for publication in the **Proceedings of M.R.S. Fall Meeting**; symposium JJ: "Nondestructive Characterisation of Materials in Aging Systems" (in press).

Barpi, F. and Valente, S. (1998a) Size-effects induced bifurcation phenomena during multiple cohesive crack propagation. **Int. J. Solids Struct.**, 35, 1851-1861.